PHYSICS

Preempting fermion sign problem: Unveiling quantum criticality through nonequilibrium dynamics in imaginary time

Yin-Kai Yu[1,2,3,4], Zhi-Xuan Li[1,2], Shuai Yin[1,2]*, Zi-Xiang Li[3,4]*

The notorious fermion sign problem, arising from fermion statistics, presents a fundamental obstacle to the numerical simulation of quantum many-body systems. Here, we introduce a framework that circumvents the sign problem in the studies of quantum criticality and its associated phases by leveraging imaginary-time nonequilibrium critical dynamics. We demonstrate that the critical properties can be accurately determined from the system's short-time relaxation, a regime where the sign problem remains manageable for quantum Monte Carlo simulations. After validating this approach on two benchmark fermionic models, we apply it to the sign-problematic Hubbard model hosting SU(3)-symmetric Dirac fermions. We present the first numerically exact characterization of its quantum phase diagram, revealing a continuous transition between a Dirac semimetal and a SU(3)-antiferromagnetic phase. This transition defines an unconventional Gross-Neveu universality class that fundamentally reshapes current understanding of Gross-Neveu criticality. Our work provides a powerful tool for investigating sign-problematic systems and quantum criticality.

INTRODUCTION

The complex sign structure of the quantum mechanical wave functions presents a central dichotomy in many-body physics. On the one hand, it endows fertile exotic phenomena across condensed matter (*1*, *2*) and high energy physics (*3*). Quantum Monte Carlo (QMC) is among the most important theoretical approaches to study the strongly correlated quantum many-body systems (*4*–*6*), offering numerically exact and unbiased solutions. On the other hand, the sign structure results in the notorious sign problem (*7*–*11*), which considerably plagues the application of QMC to investigating interacting models potentially featuring intriguing physics, including the Hubbard model at generic filling (*12*, *13*) and the lattice QCD at finite baryon density (*14*). Because the general solution of the sign problem is lacking and nondeterministic polynomial hard (*9*), developing generic strategies to circumvent or mitigate it will definitely provoke notable advances in the realm of quantum many-body physics (*15*–*36*).

Among various exotic phenomena in quantum many-body systems, quantum criticality emerges as a particularly crucial and fascinating one. The underlying physics of the quantum critical point (QCP) lays the foundation for achieving a unified theoretical framework to characterize different phases and phase transitions (*37*–*41*). Moreover, quantum criticality is intimately associated with fundamentally important phenomena in condensed matter physics such as high-T_c superconductivity (*42*–*44*) and strange metallicity (*45*, *46*). The understanding of the QCP in a nonperturbative way is severely hindered by the sign problem likewise.

Here, we propose a general framework to preempt the sign problem in QMC and unveil the quantum criticality and associated ground-state phase diagram. It is widely acknowledged that fathoming the nonequilibrium properties in quantum many-body systems is substantially more challenging than equilibrium ones. However, we leverage the nonequilibrium behavior and demonstrate that the short-time critical dynamics, which was first proposed in classical systems (*47*) and used to detect the classical critical behaviors (*48*) and then generalized to imaginary-time dynamics of QCP (*49*), provides an ingenious strategy to reliably probe quantum criticality in the presence of the sign problem, as illustrated in Fig. 1A. The underlying mechanism is that, in the short-time stage of imaginary-time relaxation for some typical initial states, (i) universal scaling behaviors manifesting the quantum criticality appear (*49*, *50*); and (ii) the sign problem remains mild in this stage, such that the reliable results are accessible by QMC simulation. Hence, bestowing the scaling of short-time dynamics (*47*–*50*), we can accurately determine the location and critical properties of the QCP, while the sign problem therein, whose severity generally increases exponentially with the imaginary time (*9*, *51*, *52*), is largely alleviated compared with the equilibrium one involving long-imaginary-time evolution.

In the following, we demonstrate the framework by studying two typical interacting fermionic models featuring Dirac QCP. We unambiguously show that accurate critical properties can be accessed through short-imaginary-time dynamics, despite the presence of the sign problem. We adopt the approach to investigate a paradigmatic strongly interacting model hosting Dirac fermions with SU(3) symmetry, which is sign problematic in any known algorithm. We establish the ground-state phase diagram of the model and reveal the critical properties of the quantum phase transition between the Dirac semimetal (DSM) and a λ_8-antiferromagnetic (AFM) phase. Intriguingly, the QCP defines an unconventional Gross-Neveu transition that goes beyond the previous paradigms of O(N) ordering, distinct from the known universality classes of Gross-Neveu transition.

RESULTS

Theoretical framework

We consider the imaginary-time relaxation dynamics for which the wave function $|\psi(\tau)\rangle$ evolves according to the imaginary-time Schrödinger equation $-\frac{\partial}{\partial\tau}|\psi(\tau)\rangle = H|\psi(\tau)\rangle$ imposed by the

[1]School of Physics, Sun Yat-sen University, Guangzhou 510275, China. [2]Guangdong Provincial Key Laboratory of Magnetoelectric Physics and Devices, Sun Yat-sen University, Guangzhou 510275, China. [3]Beijing National Laboratory for Condensed Matter Physics and Institute of Physics, Chinese Academy of Sciences, Beijing 100190, China. [4]University of Chinese Academy of Sciences, Beijing 100049, China. *Corresponding author. Email: yinsh6@mail.sysu.edu.cn (S.Y.); zixiangli@iphy.ac.cn (Z.-X.L.)

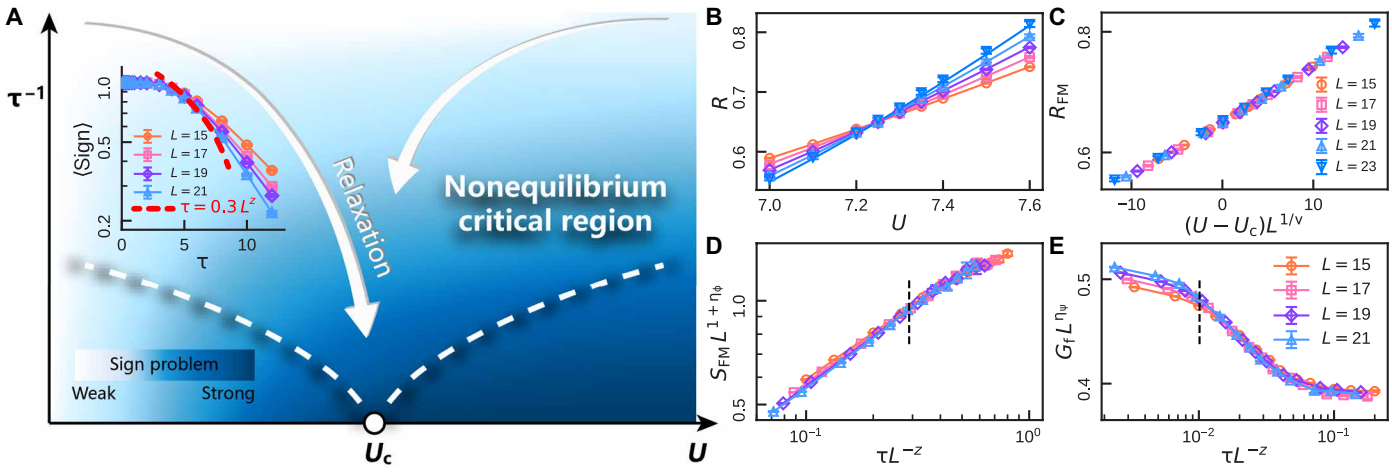

Fig. 1. Scheme of preempting sign problem to probe quantum criticality via short-time critical dynamics and the application in single-Dirac-fermion Hubbard model. (**A**) With some typical initial states, scaling behaviors governed by the QCP are reflected in the short-time stage, in which the sign problem is still weak as shown in the inset. The white dashed line indicates the nonequilibrium critical region associated with the QCP. The red dashed line in the inset indicates the average sign at $\tau = 0.3L^z$, where $z = 1$ due to the nature of the Dirac QCP. (**B**) Determination of QCP as $U_c = 7.220(37)$ via the intersection points of curves of the correlation length ratio R_{FM} versus U for different sizes at $\tau = 0.3L^z$ with DSM initial state. (**C**) Determination of $1/\nu = 1.18(3)$ by scaling collapse of R_{FM} versus rescaled $(U - U_c)$, with a reduced chi-squared value $\chi^2_\nu = 1.824$ indicating good quality. (**D**) Determination of $\eta_\phi = 0.33(2)$ via scaling collapse of curves of the structure factor S_{FM} versus rescaled τ at U_c, with $\chi^2_\nu = 0.606$. (**E**) Determination of $\eta_\psi = 0.135(2)$ via scaling collapse of curves of the fermion correlation G_f versus rescaled τ at U_c, with $\chi^2_\nu = 1.241$. The dashed lines in (D) and (E) indicate the boundary of the nonequilibrium scaling region; only the regions to the right are included in the scaling collapse analysis (see Supplementary Materials section S2B for details).

normalization condition. As its long-time solution is the ground state, this equation forms the basis of the zero-temperature projector QMC (PQMC) method, which provides a routine approach to accessing ground-state properties in numerical computations (see Supplementary Materials section S1) (*51*, *53*, *54*). Moreover, near the QCP, it was shown that universal scaling behaviors manifest themselves not only at the ground state but also in the imaginary-time relaxation process. Particularly, with initial states corresponding to the fixed points of scale transformation, after a transient nonuniversal time scale, the short-imaginary-time dynamics of observable O satisfies the following scaling form (*49*, *50*)

$$O(\tau, g, L) = L^{-\kappa} f_O\left(gL^{\frac{1}{\nu}}, \tau L^{-z}\right) \quad (1)$$

where L is linear system size and g is the distance to the critical point, κ is the scaling dimension of O, and ν is the correlation-length exponent, and z is the dynamical exponent that is generally one in the Dirac QCP. Note that all critical exponents in Eq. 1 are controlled by the QCP in the ground state. Accordingly, from Eq. 1, one can achieve the location of QCP and critical properties from the expectation value of O in the relaxation process. This nonequilibrium approach is notably different from the conventional PQMC that requires that the ground state should be determined through the evolution of long imaginary time (see Supplementary Materials section S1) (*51*, *53*, *54*). Because, in general, the severity of the sign problem exponentially increases with imaginary time in QMC (*9*, *52*), the sign problem in the short-time stage of relaxation is significantly mitigated compared with the direct simulation on ground-state properties, thereby enabling the large-scale QMC simulation with high accuracy despite the presence of the sign problem. In the following, we elucidate the theoretical framework by systematically studying several representative models with the sign problem.

Single-Dirac-fermion Hubbard model

We first consider the SLAC fermion Hubbard model with the Hamiltonian (*55*–*57*)

$$H = \sum_{i,R} t_R c^\dagger_{i\uparrow} c_{i+R\downarrow} + \text{h.c.} + U \sum_i \left(n_{i\uparrow} - \frac{1}{2}\right)\left(n_{i\downarrow} - \frac{1}{2}\right)$$

where $t_R = \frac{i(-1)^{R_x}}{\frac{L}{\pi}\sin\pi\frac{R_x}{L}}\delta_{R_y,0} + \frac{(-1)^{R_y}}{\frac{L}{\pi}\sin\pi\frac{R_y}{L}}\delta_{R_x,0}$ is the amplitude of long-range hopping on the square lattice and U is the strength of repulsive interaction. The model is sign problematic in any known QMC algorithm. Nonetheless, because the sign problem is relatively benign, a previous QMC study reveals a chiral Ising QCP separating the DSM phase and ferromagnetic (FM) phase (*55*).

Here, we present the procedure for unraveling the critical properties via the short-imaginary-time scaling of the observable as dictated in Eq. 1. In conventional PQMC, long-imaginary-time evolution is typically required (see Supplementary Materials section S1) (*51*, *53*, *54*), resulting in the severe sign problem exponentially increasing with τ, as shown in the inset of Fig. 1A. We overcome this critical difficulty by leveraging short-imaginary-time critical relaxation dynamics, with the DSM state chosen as the initial state for the following demonstration. To determine the critical point via Eq. 1, we consider observable O as the dimensionless correlation length ratio R_{FM} for the FM order (see Supplementary Materials section S2 for the detailed definition). We take a short-imaginary-time length $\tau = 0.3L^z$, where Eq. 1 reduces to $R_{FM} = f_R\left(gL^{1/\nu}\right)$. Here, the dynamical exponent is $z = 1$ for the Dirac QCP, and our framework can also determine z when unknown (see Supplementary Materials section S2), without any prior knowledge. We show the numerical results in Fig. 1B, in which the crossing point of R_{FM} versus U for different L precisely reveals a quantum phase transition from DSM to FM phase occurring at $U_c = 7.220(37)$. This analysis fully aligns with the standard procedure of finite-size scaling, given the fixed relation $\tau = 0.3L^z$.

We then perform data collapse analysis of R_{FM} for different L versus $(U-U_c)L^{1/\nu}$ and achieve accurate critical exponent $1/\nu = 1.18(3)$, as shown in Fig. 1C. Furthermore, fixing $U = U_c$, we calculate the imaginary-time evolution of FM structure order S_{FM} and fermion correlation G_f (defined in Supplementary Materials section S2), whose scaling dimensions are $(1+\eta_\phi)$ and η_ψ, respectively (*50*, *55*). By making the rescaled curves of $S_{FM}L^{(1+\eta_\phi)}$ and $G_fL^{\eta_\psi}$ versus τL^{-z} for different L collapse according to Eq. 1 as shown in Fig. 1 (D and E), we achieve the anomalous dimensions of the order parameter boson $\eta_\phi = 0.36(3)$ and the Dirac fermion $\eta_\psi = 0.134(3)$, respectively.

The choice of the initial state and the imaginary-time length are two pivotal handles in our framework. Within the nonequilibrium scaling region near the QCP, the universal scaling form (Eq. 1) and the resulting critical point and exponents are independent of these choices, while the severity of the sign problem is sensitive to them. Flexible choices of the initial state and imaginary-time length not only help alleviate the sign problem to the greatest extent but also provide a self-consistency check for the accuracy of the extracted critical point and exponents. In the demonstration shown in Fig. 1 (B and C), we used the DSM initial state with $\tau = 0.3L^z$ to locate the critical point. The same result can be reproduced by changing τ to $\tau = 0.5L^z$ or by switching the initial state to the FM state. Moreover, the scaling collapses in Fig. 1 (D and E) confirm that the system has entered the nonequilibrium scaling region. The details of self-consistency checks for different initial states and τ are provided in Supplementary Materials section S2B. Beyond the self-consistency checks, our estimates of the critical point and exponents are also approximately consistent with previous results from Gutzwiller QMC (*55*) and functional renormalization group (*58*). The substantial mitigation of the sign problem enables us to simulate larger system sizes up to $L = 23$, yielding reliable results (a systematic discussion is given in Supplementary Materials section S1E). Consequently, we unambiguously demonstrate that short-imaginary-time dynamics via QMC simulation offers a powerful approach to determine the phase transition point and critical exponents in sign-problematic strongly interacting models in a self-consistent, accurate, and unbiased manner, without relying on any prior knowledge.

Spinless *t-V* model

To further demonstrate the framework of our approach, we study another typical interacting Dirac-fermion model, termed as honeycomb spinless *t-V* model, with the Hamiltonian (*17*, *59*–*61*)

$$H = -t\sum_{\langle ij\rangle} c_i^\dagger c_j + V\sum_{\langle ij\rangle}\left(n_i-\frac{1}{2}\right)\left(n_j-\frac{1}{2}\right) \quad (2)$$

where t is nearest-neighbor (NN) hopping amplitude and V denotes the strength of NN density interaction. The appearance of the sign problem in Eq. 2 depends on the channel of Hubbard-Strotonovich (H-S) transformation. Hence, the model provides a genuine platform to confirm the accuracy and feasibility of our approach to unravel QCP in the presence of the sign problem. Previous sign-free QMC studies, with the H-S transformation in the hopping channel, reveal the critical properties of the QCP separating DSM and charge-density-wave (CDW) phases (*60*). Here, we decouple the interaction in the sign-problematic density channel (*62*) and study the QCP via short-imaginary-time relaxation dynamics.

The procedure is the same as in the previous section, but, here, we demonstrate the case with the CDW initial state. The consistency check with the DSM initial state is provided in Supplementary Materials section S3. We fix $\tau = 0.3L^z$ and determine QCP from the crossing point of curves of correlation-length ratio R_{CDW} versus V (R_{CDW} is defined in Supplementary Materials section S3), as displayed in Fig. 2A, giving rise to $V_c = 1.35(1)$. The scaling collapse analysis determines the value of ν as $1/\nu = 1.30(18)$. Additionally, the anomalous dimensions $\eta_\phi = 0.49(5)$ and $\eta_\psi = 0.073(4)$ are obtained from the evolution of the CDW structure factor S_{CDW} and the fermion correlation G_f (defined in Supplementary Materials section S3), respectively, at V_c. Both V_c and η_ϕ are consistent with previous numerical results (*58*–*60*). Notably, η_ψ is numerically determined, aligning consistently with the previous results of the functional renormalization group (*58*). These results for the model in Eq. 2 further establish the feasibility of the approach based on short-imaginary-time dynamics in accessing the critical properties, even in the presence of the sign problem. The ability to select different initial states also offers valuable benchmarks, thereby further solidifying the reliability of our approach.

SU(3) Hubbard model

Building on the successful application of our method to previous models, we now apply it to systematically investigate the unexplored sign-problematic systems. Our particular interest lies in identifying an exotic Dirac QCP belonging to a previously unidentified universality class. To this end, we consider SU(3) Hubbard model on square lattice with staggered magnetic flux, described by the following Hamiltonian

$$H = -\sum_{\langle ij\rangle\alpha} t_{ij}c_{i\alpha}^\dagger c_{j\alpha} + \frac{U}{2}\sum_i\left(\sum_\alpha n_{i\alpha}-\frac{3}{2}\right)^2 \quad (3)$$

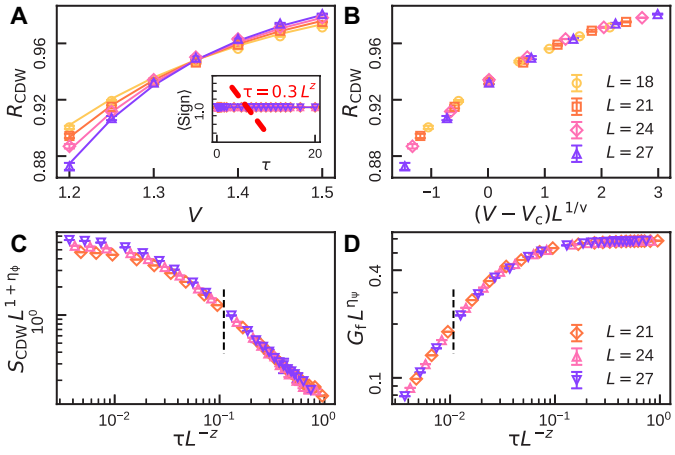

Fig. 2. Probing quantum criticality via short-imaginary-time critical dynamics in spinless *t-V* model with CDW initial state. (**A**) Determination of QCP as $V_c = 1.35(1)$ via the intersection points of R_{CDW} versus V for different L at $\tau = 0.3L^z$, where $z = 1$. Shown in the inset is the evolution of average sign with red dashed curve marks $\tau = 0.3L^z$. (**B**) Determination of $1/\nu = 1.30(18)$ via scaling collapse of R_{CDW} versus rescaled $(V-V_c)$, with $\chi_\nu^2 = 1.518$ demonstrating the collapse quality. (**C** and **D**) Determination of $\eta_\phi = 0.49(5)$ and $\eta_\psi = 0.073(4)$ via scaling collapse of the short-imaginary-time dynamics of S_{CDW} and G_f versus rescaled τ, respectively, with $\chi_\nu^2 = 1.668$ and 0.963 demonstrating the collapse quality in the nonequilibrium scaling region to the right of the dashed lines.

where $\alpha = 1, 2,$ and 3 is the flavor index of fermion; U is repulsive Hubbard interaction strength; and $t_{ij} = te^{i\theta_{ij}}$, in which $t = 1$, is set as energy unit. As illustrated in Fig. 3A, the magnetic flux in each plaquette is $\sum_{\square}\theta_{ij} = (-1)^{i_x+i_y}\phi$. For $\phi = 0$ cases, recent constrained-path QMC and finite-temperature determinant QMC studies have investigated the model at $^1/_3$ filling (*63*, *64*). For nonzero ϕ, the energy dispersion of Eq. 3 in the noninteracting limit features two Dirac points located at momenta $\left(\pm\frac{\pi}{2}, \pm\frac{\pi}{2}\right)$, as shown in the inset of Fig. 3A. We fix our simulation at half-filling such that the Fermi level is located at the Dirac points. The model in Eq. 3 respects $SU(3) \times Z_2$ symmetry, where SU(3) is the rotation symmetry in flavor space and Z_2 is the sublattice symmetry that exchanges the two sublattices on the staggered-flux square lattice with each unit cell containing two sites.

The SU(N) symmetry plays overarching roles in modern physics. For instance, the SU(3) symmetry lays the foundation for strong interaction between quarks (*3*). Recently, interacting fermionic models with SU(N) symmetry have been realized in optical lattice (*65*, *66*). Extensive theoretical and numerical efforts, including QMC simulations, are devoted to understanding the exotic phenomena arising from the interplay between strong interaction, Dirac fermions, and multiflavor physics (*67*–*71*). However, despite its fundamental importance, unbiased numerical studies on SU(N)-symmetric model with repulsive interaction for odd N are scarce, primarily due to the notorious sign problem. Hence, we implement our approach to preempt the sign problem and unravel the quantum phases and exotic QCP in Eq. 3, a paradigmatic interacting model for odd N SU(N) symmetry.

Before embarking on QMC simulation, we perform a mean-field calculation to detect the feature of the ground state schematically. The mean-field calculation shows that an AFM order is favored by the strong Hubbard interaction (see Supplementary Materials section S4). The order parameter is characterized in terms of the generators of SU(3) symmetry group, which is expressed by the eight Gell-Mann matrices in flavor space for convenience (*72*) [the details of the SU(3) algebra are introduced in the Supplementary Materials]. In stark contrast to the case of SU(2), only one Gell-Mann matrix is full rank without zero eigenvalue, dubbed as $\lambda_8 = \mathrm{diag}\left(\frac{1}{\sqrt{3}}, \frac{1}{\sqrt{3}}, -\frac{2}{\sqrt{3}}\right)$. Consequently, for the AFM order in SU(3) fermions, only the order parameter associated with λ_8 is the mass term fully opening spectral gap in Dirac fermions, which is expressed as $m_{\lambda_8-\mathrm{AFM}} = \frac{1}{L^2}\sum_{i,\alpha,\beta} c^{\dagger}_{i\alpha}\lambda_8^{\alpha\beta}c_{i\beta}(-1)^{i_x+i_y}$. The mean-field calculation also confirms that such AFM order is energetically favorable in the model in Eq. 3 (see Supplementary Materials section S4).

In the λ_8-AFM ordered phase, the Z_2 sublattice symmetry is broken and the SU(3) symmetry is broken into SU(2) × U(1) (see Supplementary Materials section S4D for details), as illustrated in Fig. 3A. This order parameter transforms under the adjoint representation of SU(3), spanning the vacuum manifold $\frac{SU(3)\times Z_2}{SU(2)\times U(1)}$. Such symmetry breaking defines a new unconventional Gross-Neveu QCP, where the order parameter symmetry is SU(3), in contrast to the O(N) order parameters of the conventional Gross-Neveu universality classes such as chiral Ising, chiral XY, and chiral Heisenberg.

To reveal the critical properties, we perform short-time QMC simulation starting from a fully ordered state at $\phi = 0.075\pi$ and $\tau L^{-z} = 0.25$ ($z = 1$). The results of correlation length ratio $R_{\lambda_8-\mathrm{AFM}}$ for λ_8-AFM order (defined in Supplementary Materials section S4) are shown in Fig. 3B, and the crossing points dictate the phase transition point from DSM to λ_8-AFM phase occurring at $U_c = 1.10(5)$. We also compute the correlation-length ratios for other types of AFM order instead of λ_8, confirming that only λ_8-AFM long-range order is present in the ground state (see Supplementary Materials section S4). With varying magnetic flux ϕ, we apply the same procedure to map out the ground-state phase diagram of Eq. 3, as shown in Fig. 3A, in which U_c increases with ϕ.

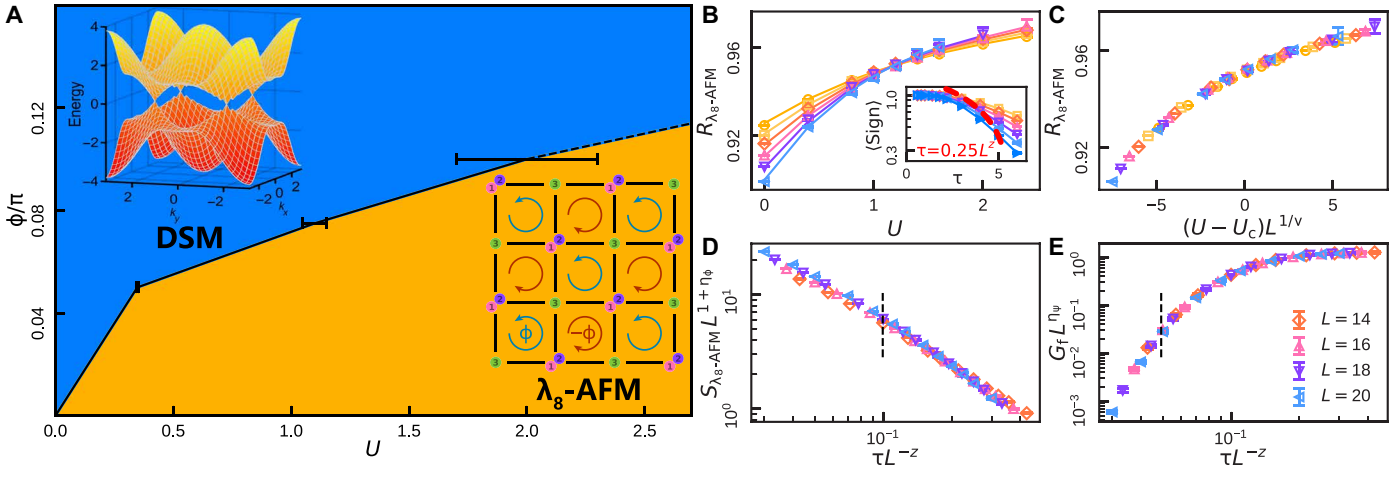

Fig. 3. Phase diagram and quantum criticality in SU(3) Hubbard model detected by short-imaginary-time dynamics with λ_8-AFM initial state. (**A**) Phase diagram determined via short-imaginary-time dynamics. Insets show the energy spectra of DSM state (top left) and sketch of λ_8-AFM order in which a fermion with one flavor (green "3") is situated at one sublattice and double fermions with the other two flavors (pink "1" and violet "2") are situated at the other sublattice (bottom right). (**B** and **C**) Critical point $U_c = 1.10(5)$ for $\phi = 0.075\pi$ and $1/\nu = 0.68(5)$ determined via curves of $R_{\lambda_8-\mathrm{AFM}}$ versus U for different L at $\tau = 0.25L^z$, where $z = 1$ and $\chi^2_\nu = 1.239$ for the collapse quality. Shown in the inset of (B) is the evolution of average sign with red dashed curve marks $\tau = 0.25L^z$. (**D** and **E**) $\eta_\phi = 0.55(5)$ and $\eta_\psi = 0.15(3)$ determined via the scaling collapse of evolution curves of $S_{\lambda_8-\mathrm{AFM}}$ and G_f, respectively, with $\chi^2_\nu = 1.382$ and $\chi^2_\nu = 0.560$ demonstrating the collapse quality in the nonequilibrium scaling region to the right of the dashed lines.

After accessing the phase diagram, we investigate the critical properties. The data collapse analysis of $R_{\lambda_8-\mathrm{AFM}}$ versus $(U-U_c)L^{1/\nu}$ in the regime close to QCP with fixed $\phi = 0.075$ gives $1/\nu = 0.68(5)$, as shown in Fig. 3C. Moreover, at U_c, the short-imaginary-time dynamics of the structure factor $S_{\lambda_8-\mathrm{AFM}}$ and the fermion correlation function G_f (defined in Supplementary Materials section S4) yield $\eta_\phi = 0.55(5)$ and $\eta_\psi = 0.15(3)$, as presented in Fig. 3 (D and E), respectively. To confirm the universality of this phase transition, we also evaluate the critical exponents for other values of ϕ, as presented in the Supplementary Materials, and they are mutually consistent within error bars. The critical exponents found here are numerically distinct from those of any conventional Gross-Neveu universality class (*73*, *74*) (for comparison, see the Supplementary Materials), providing conclusive evidence that this transition belongs to a new universality class.

DISCUSSION

In summary, we introduce an innovative theoretical framework unraveling ground-state properties, with a particular focus on quantum criticality, in quantum many-body systems. Our method effectively circumvents the notorious sign problem in QMC by leveraging the short-stage imaginary-time relaxation dynamics. We provide compelling evidence of its accuracy and efficiency across several strongly interacting models, showcasing a marked reduction in computational cost compared to conventional equilibrium QMC. For example, the estimate time for the SU(3) Hubbard model with $L = 10$ is billions of times shorter with our approach than with equilibrium PQMC (see Supplementary Materials section S4). Furthermore, the inherent flexibility in choosing initial states, coupled with a robust scaling relation, provides a crucial benchmark for ensuring accuracy within our framework. Besides, this approach can distinguish between first-order and continuous phase transitions (see Supplementary Materials section S1). This work, therefore, establishes a powerful strategy for the unbiased numerical study of the exotic quantum phases and quantum phase transitions in a broad class of previously computationally inaccessible systems.

More intriguingly, we leverage our newly developed approach to make a pioneering investigation into the SU(3) repulsive Hubbard model hosting Dirac fermions. This study presents the unprecedented characterization of the ground-state phase diagram and the QCP in the SU(N) repulsive Hubbard model with odd N using unbiased numerical approaches. We identify the example of Gross-Neveu QCP that fundamentally differs from the conventional ones typically confined to the chiral O(N) universality classes (see Supplementary Materials section S4). Moreover, the critical properties are potentially detectable in the synthetic quantum simulators such as optical lattice of cold atoms (*65*, *66*). Hence, our findings on the SU(3) Hubbard model not only establish a significant novel direction in modern statistics physics for exploring the fermionic QCP but also offer critical theoretical guidance for the forthcoming experimental exploration of exotic physics in strongly correlated SU(N) fermionic models.

Our innovative approach presents a powerfully generalizable framework, extending readily to other fermionic QCP, including the notoriously challenging metallic QCP involving Fermi surfaces, whose critical properties are of immense theoretical and experimental interest but have remained largely inscrutable. Moreover, the short-time nonequilibrium QMC is also applicable to sign-problematic bosonic models, opening entirely new avenues. We carefully delineate the boundaries of our method: It is not a fully generalized solution to the sign problem. Arbitrarily short evolution times retain excessive memory of the initial state, preventing evolution into the desired nonequilibrium scaling regime (see Supplementary Materials section S1 for detailed discussions). This means a mild sign problem ensuring accurate results within the short-time nonequilibrium scaling regime cannot be universally guaranteed for every model. For instance, in the SU(3) Hubbard model with large staggered magnetic flux, the sign problem remains too severe for highly accurate results near the QCP, even in the short-time stage. Despite these limitations, the framework's flexibility allows for future efficiency enhancements, such as through improvement of initial state and optimization of H-S channel (*31*, *32*). This work is not merely an incremental improvement; it delivers a novel pathway toward establishing a general and unbiased numerical strategy for unraveling the mysteries of the ground-state phase diagram and QCP in strongly correlated systems, a long-sought goal in the field.

Supplementary Materials

This PDF file includes:

Sections S1 to S4
Figs. S1 to S19
Tables S1 to S5
References

REFERENCES

1. S. Sachdev, *Quantum Phase Transitions* (Cambridge Univ. Press, ed. 2, 2011); https://doi.org/10.1017/CBO9780511973765.
2. J. Zaanen, Quantum critical electron systems: The uncharted sign worlds. *Science* **319**, 1205–1207 (2008).
3. S. Weinberg, *The Quantum Theory of Fields* (Cambridge Univ. Press, 2013), vol. 1.
4. R. Blankenbecler, D. J. Scalapino, R. L. Sugar, Monte Carlo calculations of coupled boson-fermion systems. I. *Phys. Rev. D* **24**, 2278–2286 (1981).
5. J. E. Hirsch, D. J. Scalapino, R. L. Sugar, R. Blankenbecler, Efficient Monte Carlo procedure for systems with fermions. *Phys. Rev. Lett.* **47**, 1628–1631 (1981).
6. J. E. Hirsch, Two-dimensional Hubbard model: Numerical simulation study. *Phys. Rev. B* **31**, 4403–4419 (1985).
7. E. Y. Loh, J. E. Gubernatis, R. T. Scalettar, S. R. White, D. J. Scalapino, R. L. Sugar, Sign problem in the numerical simulation of many-electron systems. *Phys. Rev. B* **41**, 9301–9307 (1990).
8. P. Henelius, A. W. Sandvik, Sign problem in Monte Carlo simulations of frustrated quantum spin systems. *Phys. Rev. B* **62**, 1102–1113 (2000).
9. M. Troyer, U.-J. Wiese, Computational complexity and fundamental limitations to fermionic quantum Monte Carlo simulations. *Phys. Rev. Lett.* **94**, 170201 (2005).
10. M. B. Hastings, How quantum are non-negative wavefunctions? *J. Math. Phys.* **57**, 015210 (2016).
11. Z. Ringel, D. L. Kovrizhin, Quantized gravitational responses, the sign problem, and quantum complexity. *Sci. Adv.* **3**, e1701758 (2017).
12. D. P. Arovas, E. Berg, S. A. Kivelson, S. Raghu, The Hubbard model. *Annu. Rev. Condens. Matter Phys.* **13**, 239–274 (2022).
13. M. Qin, T. Schäfer, S. Andergassen, P. Corboz, E. Gull, The Hubbard model: A computational perspective. *Annu. Rev. Condens. Matter Phys.* **13**, 275–302 (2022).
14. T. DeGrand, C. DeTar, *Lattice Methods for Quantum Chromodynamics* (World Scientific, 2006); https://doi.org/10.1142/6065.
15. Z.-X. Li, H. Yao, Sign-problem-free fermionic quantum Monte Carlo: Developments and applications. *Annu. Rev. Condens. Matter Phys.* **10**, 337–356 (2019).
16. S. Chandrasekharan, U.-J. Wiese, Meron-cluster solution of fermion sign problems. *Phys. Rev. Lett.* **83**, 3116–3119 (1999).
17. E. F. Huffman, S. Chandrasekharan, Solution to sign problems in half-filled spin-polarized electronic systems. *Phys. Rev. B* **89**, 111101 (2014).
18. C. Wu, S.-C. Zhang, Sufficient condition for absence of the sign problem in the fermionic quantum Monte Carlo algorithm. *Phys. Rev. B* **71**, 155115 (2005).
19. E. Berg, M. A. Metlitski, S. Sachdev, Sign-problem-free quantum Monte Carlo of the onset of antiferromagnetism in metals. *Science* **338**, 1606–1609 (2012).

20. Z.-X. Li, Y.-F. Jiang, H. Yao, Solving the fermion sign problem in quantum Monte Carlo simulations by Majorana representation. *Phys. Rev. B* **91**, 241117 (2015).
21. Z.-X. Li, Y.-F. Jiang, H. Yao, Majorana-time-reversal symmetries: A fundamental principle for sign-problem-free quantum Monte Carlo simulations. *Phys. Rev. Lett.* **117**, 267002 (2016).
22. S. Zhang, H. Krakauer, Quantum Monte Carlo method using phase-free random walks with slater determinants. *Phys. Rev. Lett.* **90**, 136401 (2003).
23. L. Wang, Y.-H. Liu, M. Iazzi, M. Troyer, G. Harcos, Split orthogonal group: A guiding principle for sign-problem-free fermionic simulations. *Phys. Rev. Lett.* **115**, 250601 (2015).
24. Z. C. Wei, C. Wu, Y. Li, S. Zhang, T. Xiang, Majorana positivity and the fermion sign problem of quantum Monte Carlo simulations. *Phys. Rev. Lett.* **116**, 250601 (2016).
25. R. Mondaini, S. Tarat, R. T. Scalettar, Quantum critical points and the sign problem. *Science* **375**, 418–424 (2022).
26. D. Hangleiter, I. Roth, D. Nagaj, J. Eisert, Easing the Monte Carlo sign problem. *Sci. Adv.* **6**, eabb8341 (2020).
27. R. Levy, B. K. Clark, Mitigating the sign problem through basis rotations. *Phys. Rev. Lett.* **126**, 216401 (2021).
28. Z.-Y. Han, Z.-Q. Wan, H. Yao, Pfaffian quantum Monte Carlo: Solution to Majorana sign ambiguity and applications. arXiv:2408.10311 [cond-mat.str-el] (2024).
29. A. Alexandru, G. Başar, P. F. Bedaque, N. C. Warrington, Complex paths around the sign problem. *Rev. Mod. Phys.* **94**, 015006 (2022).
30. O. Golan, A. Smith, Z. Ringel, Intrinsic sign problem in fermionic and bosonic chiral topological matter. *Phys. Rev. Res.* **2**, 043032 (2020).
31. W.-X. Chang, Z.-X. Li, Boosting quantum Monte Carlo and alleviating sign problem by gutzwiller projection. *Phys. Rev. B* **110**, 085152 (2024).
32. Z.-Q. Wan, S.-X. Zhang, H. Yao, Mitigating the fermion sign problem by automatic differentiation. *Phys. Rev. B* **106**, L241109 (2022).
33. X. Zhang, G. Pan, X. Y. Xu, Z. Y. Meng, Fermion sign bounds theory in quantum Monte Carlo simulation. *Phys. Rev. B* **106**, 035121 (2022).
34. T. Sato, F. F. Assaad, Quantum Monte Carlo simulation of generalized kitaev models. *Phys. Rev. B* **104**, L081106 (2021).
35. M.-S. Vaezi, A.-R. Negari, A. Moharramipour, A. Vaezi, Amelioration for the sign problem: An adiabatic quantum Monte Carlo algorithm. *Phys. Rev. Lett.* **127**, 217003 (2021).
36. O. Grossman, E. Berg, Robust fermi-liquid instabilities in sign problem-free models. *Phys. Rev. Lett.* **131**, 056501 (2023).
37. S. L. Sondhi, S. M. Girvin, J. P. Carini, D. Shahar, Continuous quantum phase transitions. *Rev. Mod. Phys.* **69**, 315–333 (1997).
38. M. Vojta, Quantum phase transitions. *Rep. Prog. Phys.* **66**, 2069–2110 (2003).
39. J. A. Hertz, Quantum critical phenomena. *Phys. Rev. B* **14**, 1165–1184 (1976).
40. A. J. Millis, Effect of a nonzero temperature on quantum critical points in itinerant fermion systems. *Phys. Rev. B* **48**, 7183–7196 (1993).
41. E. Berg, S. Lederer, Y. Schattner, S. Trebst, Monte Carlo studies of quantum critical metals. *Annu. Rev. Condens. Matter Phys.* **10**, 63–84 (2019).
42. D. J. Scalapino, A common thread: The pairing interaction for unconventional superconductors. *Rev. Mod. Phys.* **84**, 1383–1417 (2012).
43. P. A. Lee, N. Nagaosa, X.-G. Wen, Doping a mott insulator: Physics of high-temperature superconductivity. *Rev. Mod. Phys.* **78**, 17–85 (2006).
44. S. Lederer, Y. Schattner, E. Berg, S. A. Kivelson, Enhancement of superconductivity near a nematic quantum critical point. *Phys. Rev. Lett.* **114**, 097001 (2015).
45. C. M. Varma, Colloquium: Linear in temperature resistivity and associated mysteries including high temperature superconductivity. *Rev. Mod. Phys.* **92**, 031001 (2020).
46. P. W. Phillips, N. E. Hussey, P. Abbamonte, Stranger than metals. *Science* **377**, eabh4273 (2022).
47. H. K. Janssen, B. Schaub, B. Schmittmann, New universal short-time scaling behaviour of critical relaxation processes. *Z. Phys. B Condens. Matter* **73**, 539–549 (1989).
48. Z. B. Li, L. Schülke, B. Zheng, Dynamic Monte Carlo measurement of critical exponents. *Phys. Rev. Lett.* **74**, 3396–3398 (1995).
49. S. Yin, P. Mai, F. Zhong, Universal short-time quantum critical dynamics in imaginary time. *Phys. Rev. B* **89**, 144115 (2014).
50. Y.-K. Yu, Z. Zeng, Y.-R. Shu, Z.-X. Li, S. Yin, Nonequilibrium dynamics in Dirac quantum criticality. arXiv:2310.10601 [cond-mat.str-el] (2023).
51. F. Assaad, H. Evertz, *World-Line and Determinantal Quantum Monte Carlo Methods for Spins, Phonons and Electrons* (Springer, 2008), pp. 277–356.
52. V. I. Iglovikov, E. Khatami, R. T. Scalettar, Geometry dependence of the sign problem in quantum Monte Carlo simulations. *Phys. Rev. B* **92**, 045110 (2015).
53. S. Sorella, S. Baroni, R. Car, M. Parrinello, A novel technique for the simulation of interacting fermion systems. *Europhys. Lett.* **8**, 663–668 (1989).
54. S. Sorella, The Hubbard-stratonovich transformation and the Hubbard model. *Int. J. Mod. Phys. B* **5**, 937–976 (1991).
55. S. M. Tabatabaei, A.-R. Negari, J. Maciejko, A. Vaezi, Chiral ising gross-neveu criticality of a single Dirac cone: A quantum Monte Carlo study. *Phys. Rev. Lett.* **128**, 225701 (2022).
56. Z.-X. Li, A. Vaezi, C. B. Mendl, H. Yao, Numerical observation of emergent spacetime supersymmetry at quantum criticality. *Sci. Adv.* **4**, eaau1463 (2018).
57. T. C. Lang, A. M. Läuchli, Quantum Monte Carlo simulation of the chiral Heisenberg Gross-Neveu-Yukawa phase transition with a single Dirac cone. *Phys. Rev. Lett.* **123**, 137602 (2019).
58. G. P. Vacca, L. Zambelli, Multimeson Yukawa interactions at criticality. *Phys. Rev. D* **91**, 125003 (2015).
59. L. Wang, P. Corboz, M. Troyer, Fermionic quantum critical point of spinless fermions on a honeycomb lattice. *New J. Phys.* **16**, 103008 (2014).
60. Z.-X. Li, Y.-F. Jiang, H. Yao, Fermion-sign-free Majarana-quantum-Monte-Carlo studies of quantum critical phenomena of Dirac fermions in two dimensions. *New J. Phys.* **17**, 085003 (2015).
61. S. Hesselmann, S. Wessel, Thermal ising transitions in the vicinity of two-dimensional quantum critical points. *Phys. Rev. B* **93**, 155157 (2016).
62. Z.-X. Li, Z.-Q. Wan, H. Yao, Asymptotic sign free in interacting fermion models. arXiv:2211.00663 [cond-mat.str-el] (2022).
63. C. Feng, E. Ibarra-García-Padilla, K. R. A. Hazzard, R. Scalettar, S. Zhang, E. Vitali, Metal-insulator transition and quantum magnetism in the SU(3) fermi-Hubbard model. *Phys. Rev. Res.* **5**, 043267 (2023).
64. E. Ibarra-García-Padilla, C. Feng, G. Pasqualetti, S. Fölling, R. T. Scalettar, E. Khatami, K. R. A. Hazzard, Metal-insulator transition and magnetism of SU(3) fermions in the square lattice. *Phys. Rev. A* **108**, 053312 (2023).
65. H. Ozawa, S. Taie, Y. Takasu, Y. Takahashi, Antiferromagnetic spin correlation of SU(N) fermi gas in an optical superlattice. *Phys. Rev. Lett.* **121**, 225303 (2018).
66. S. Taie, E. Ibarra-García-Padilla, N. Nishizawa, Y. Takasu, Y. Kuno, H. T. Wei, R. T. Scalettar, K. R. A. Hazzard, Y. Takahashi, Observation of antiferromagnetic correlations in an ultracold SU(N) Hubbard model. *Nat. Phys.* **18**, 1356–1361 (2022).
67. T. C. Lang, Z. Y. Meng, A. Muramatsu, S. Wessel, F. F. Assaad, Dimerized solids and resonating plaquette order in SU(N)-Dirac fermions. *Phys. Rev. Lett.* **111**, 066401 (2013).
68. Z. Zhou, D. Wang, Z. Y. Meng, Y. Wang, C. Wu, Mott insulating states and quantum phase transitions of correlated SU(2N) Dirac fermions. *Phys. Rev. B* **93**, 245157 (2016).
69. Y.-Y. He, H. Q. Wu, Y. Z. You, C. Xu, Z. Y. Meng, Z. Y. Lu, Quantum critical point of Dirac fermion mass generation without spontaneous symmetry breaking. *Phys. Rev. B* **94**, 241111 (2016).
70. Z.-X. Li, Y.-F. Jiang, S.-K. Jian, H. Yao, Fermion-induced quantum critical points. *Nat. Commun.* **8**, 314 (2017).
71. H. Xu, X. Li, Z. Zhou, X. Wang, L. Wang, C. Wu, Y. Wang, Trion states and quantum criticality of attractive SU(3) Dirac fermions. *Phys. Rev. Res.* **5**, 023180 (2023).
72. M. Gell-Mann, Symmetries of baryons and mesons. *Phys. Rev.* **125**, 1067–1084 (1962).
73. B. Rosenstein, H.-L. Yu, A. Kovner, Critical exponents of new universality classes. *Phys. Lett. B* **314**, 381–386 (1993).
74. L. Janssen, I. F. Herbut, Antiferromagnetic critical point on graphene's honeycomb lattice: A functional renormalization group approach. *Phys. Rev. B* **89**, 205403 (2014).
75. S. R. White, D. J. Scalapino, R. L. Sugar, E. Y. Loh, J. E. Gubernatis, R. T. Scalettar, Numerical study of the two-dimensional Hubbard model. *Phys. Rev. B* **40**, 506–516 (1989).
76. E. S. Sørensen, M. Wallin, S. M. Girvin, A. P. Young, Universal conductivity of dirty bosons at the superconductor-insulator transition. *Phys. Rev. Lett.* **69**, 828–831 (1992).
77. Y.-R. Shu, S. Yin, D.-X. Yao, Universal short-time quantum critical dynamics of finite-size systems. *Phys. Rev. B* **96**, 094304 (2017).
78. Y.-R. Shu, S.-K. Jian, S. Yin, Nonequilibrium dynamics of deconfined quantum critical point in imaginary time. *Phys. Rev. Lett.* **128**, 020601 (2022).
79. Y. Otsuka, S. Yunoki, S. Sorella, Universal quantum criticality in the metal-insulator transition of two-dimensional interacting Dirac electrons. *Phys. Rev. X* **6**, 011029 (2016).
80. T. C. Lang, A. M. Läuchli, Chiral Heisenberg Gross-Neveu-Yukawa criticality: Honeycomb vs. SLAC fermions. arXiv:2503.15000 [cond-mat.str-el] (2025).
81. N. Read, S. Sachdev, Valence-bond and spin-Peierls ground states of low-dimensional quantum antiferromagnets. *Phys. Rev. Lett.* **62**, 1694–1697 (1989).
82. N. Read, S. Sachdev, Spin-Peierls, valence-bond solid, and Néel ground states of low-dimensional quantum antiferromagnets. *Phys. Rev. B* **42**, 4568–4589 (1990).
83. Y. Da Liao, X. Y. Xu, Z. Y. Meng, Y. Qi, Dirac fermions with plaquette interactions. ii. SU(4) phase diagram with Gross-Neveu criticality and quantum spin liquid. *Phys. Rev. B* **106**, 115149 (2022).
84. D. Wang, Y. Li, Z. Cai, Z. Zhou, Y. Wang, C. Wu, Competing orders in the 2D half-filled SU(2*n*) Hubbard model through the pinning-field quantum Monte Carlo simulations. *Phys. Rev. Lett.* **112**, 156403 (2014).
85. Z. Zhou, C. Wu, Y. Wang, Mott transition in the π-flux SU(4) Hubbard model on a square lattice. *Phys. Rev. B* **97**, 195122 (2018).
86. X. Y. Xu, Y. Qi, L. Zhang, F. F. Assaad, C. Xu, Z. Y. Meng, Monte Carlo study of lattice compact quantum electrodynamics with fermionic matter: The parent state of quantum phases. *Phys. Rev. X* **9**, 021022 (2019).
87. W. Wang, D.-C. Lu, X. Y. Xu, Y.-Z. You, Z. Y. Meng, Dynamics of compact quantum electrodynamics at large fermion flavor. *Phys. Rev. B* **100**, 085123 (2019).

88. L. Janssen, W. Wang, M. M. Scherer, Z. Y. Meng, X. Y. Xu, Confinement transition in the QED_3-Gross-Neveu-XY universality class. *Phys. Rev. B* **101**, 235118 (2020).
89. S. Han, I. F. Herbut, Gross-Neveu-Yukawa theory of SO(2*n*)→SO(*n*)×SO(*n*) spontaneous symmetry breaking. *Phys. Rev. B* **110**, 125131 (2024).
90. S. Ray, Unconventional Gross-Neveu quantum criticality: Interaction-induced SO(3)-biadjoint insulator and emergent SU(3) symmetry. *Phys. Rev. B* **109**, 165137 (2024).
91. S. Han, S. Ray, I. F. Herbut, Gross-Neveu-Yukawa SO(2) and SO(3) tensorial criticality. *Phys. Rev. B* **111**, 115131 (2025).

Acknowledgments: We acknowledge helpful discussions with Y. Pan, C. Cai, S.-H. Shi, and C.-Y. Shen. **Funding:** Y.-K.Y., Zhi-X.L., and S.Y. are supported by the National Natural Science Foundation of China (grant nos. 12222515 and 12075324).Zi-X.L. is supported by Beijing Natural Science Foundation (no. JR25007) and the National Natural Science Foundation of China (nos. 12347107 and 12474146). S.Y. is also supported by the Science and Technology Projects in Guangdong Province (grant no. 2021QN02X561) and in Guangzhou City (grant no. 2025A04J5408). **Author contributions:** Zi-X.L. and S.Y. conceived and supervised the project. Y.-K.Y. and Zhi-X.L. carried out the numerical calculations and data analysis. All authors participated in discussions and contributed to writing the manuscript. **Competing interests:** The authors declare that they have no competing interests. **Data and materials availability:** All data and code needed to evaluate and reproduce the results in the paper are present in the paper and/or the Supplementary Materials. All raw data underlying the results presented in the main text and the Supplementary Materials are archived in the Dryad Digital Repository (https://doi.org/10.5061/dryad.dncjsxmch) under the CC0 Public Domain Dedication.

Submitted 9 July 2025
Accepted 25 November 2025
Published 1 January 2026
10.1126/sciadv.adz4856